Key Engineering Materials
ISSN: 1662-9795, Vol. 1047, pp 183-190

Submitted: 2026-01-18
Accepted: 2026-02-11
Online: 2026-04-13

Effect of Deposition Strategy on Geometric Stability in Wire Arc Additive Manufacturing of Inconel 625

Eleonora Viola[1,2,a*], Alessia Teresa Silvestri[3,b] and Antonino Squillace[1,c]

[1]Department Of Chemical, Materials and Industrial Production Engineering, University of Naples Federico II, Piazzale Vincenzo Tecchio 80, 80125, Naples, Italy

[2]Department of Management, Information and Production Engineering, University of Bergamo, Via A. Einstein 2, 24044, Dalmine, Italy

[3]Department of Engineering and Sciences, Faculty of Technology and Innovation Sciences, Universitas Mercatorum, Piazza Mattei 10, 00186 Rome, Italy

[a*]eleonora.viola@unina.it, [b]alessiateresa.silvestri@unina.it, [c]squillac@unina.it

Keywords: wire arc additive manufacturing (WAAM), cold metal transfer (CMT), inconel 625, deposition strategy.

Abstract. Wire Arc Additive Manufacturing (WAAM) is a promising technology for producing large, high-performance metallic components, though process stability and geometric control remain critical challenges. The present work investigates the influence of deposition trajectory on the geometry, surface quality, and microhardness of wire arc additive manufactured Inconel 625 walls, produced by a Cold Metal Transfer (CMT) process. A conventional linear double-pass strategy is directly compared with a single-pass triangular weave trajectory under equivalent heat input per unit length, in order to isolate the effect of the torch path from other process variables. Single-layer and multi-layer walls were fabricated and characterized in terms of geometry, dimensional stability, surface waviness, and Vickers microhardness. The results show that the weave trajectory leads to improved geometric consistency, reduced variability, and significantly lower surface waviness compared to the linear strategy, while maintaining comparable mean wall width and microhardness. These findings demonstrate that appropriate trajectory design can enhance geometric stability and near-net-shape capability in WAAM-CMT without altering thermal input or material properties.

Introduction

Additive Manufacturing (AM) has emerged as a revolutionary technology within the Industry 4.0 paradigm, representing a strategic departure from traditional subtractive manufacturing processes. AM offers significant advantages, including reduced material waste and shorter lead times [1]. These capabilities have established AM as a critical manufacturing option in high-value sectors such as the aerospace, marine, nuclear, biomedical, and petrochemical industries [2].

Metal AM processes can be categorized based on feedstock form into powder-based and wire-based methods [3]. Among wire-based techniques, Wire Arc Additive Manufacturing (WAAM) has garnered significant attention. WAAM uses an electric arc to melt wire feedstock and offers distinct advantages over powder-based methods, most notably a higher material deposition rate, resulting in shorter fabrication times and lower production costs [4]. In WAAM, the choice of heat source is critical, as it directly affects the deposition rate, thermal management, and the resulting metallurgical quality of the component [5,6]. Among the available options, Cold Metal Transfer (CMT), a specialized variant of the Gas Metal Arc Welding (GMAW), has emerged as a preferred approach due to its ability to provide significantly lower heat input, which is achieved through the digital coordination of the wire feeding movement and droplet transfer [7,8].

These characteristics make WAAM a highly promising technology for the production of large, high-performance metallic components, particularly when using strategically valuable and costly materials. Inconel 625, a premier nickel-based superalloy, is often chosen for such applications. It combines excellent tensile strength at elevated temperatures, superior resistance to corrosion and

oxidation, and outstanding fatigue performance, making it indispensable for components such as gas turbine cores, subsea controllers, and chemical plant hardware [3,9].
Despite these advantages, Inconel 625 presents specific challenges in WAAM, as the final properties of the manufactured component depend not only on the material itself but critically on the process parameters [10]. Different deposition strategies generate spatially varying thermal histories, which in turn produce microstructural features that directly influence mechanical performance [4,11]. Previous studies on deposition strategies have focused on geometrical accuracy, microstructural evolution, and final mechanical performance [11,12,13]. However, many of these works vary multiple parameters simultaneously, making it difficult to isolate the specific influence of the torch path.
In this study, the effect of deposition trajectory in WAAM-CMT of Inconel 625 is systematically investigated. A conventional linear double-pass strategy is directly compared with a single-pass weave strategy under equivalent heat input, ensuring that observed differences in wall geometry and surface quality can be primarily attributed to the deposition trajectory. This approach provides a clear link between trajectory design, layer stability, and final part quality, and demonstrates how trajectory control enhances process repeatability and enables a more robust understanding of geometry evolution in WAAM-CMT processes.

Materials and Methods

Experiments were carried out using the WAAM system shown in Fig. 1, which consists of a Fronius TransPuls Synergic CMT power source, a Delta robot integrated with the welding torch, a wire feeding system, and a gas shielding system. Inconel 625 (ERNiCrMo-3) wire with a diameter of 1.0 mm was used as the filler metal, while mild steel plates with dimensions of 250 mm × 30 mm × 20 mm served as the substrate. The average chemical composition of the wire is shown in Table 1. A constant flow of 16 L/min of shielding gas (98% Argon, 2% CO_2) was used to prevent oxidation of the molten pool. The contact tip to work distance (CTWD) was maintained at 15 mm for all experiments.

Fig. 1. WAAM setup used for deposition.

Table 1. Chemical composition of Inconel 625 wire (wt%).

Cr	Mo	Nb	Fe	Co	Si	Mn	Ti	Al	C	P	S	Ni
20.0 – 23.0	8.0 – 10.0	3.15 – 4.15	≤5.0	≤1.0	≤0.50	≤0.50	≤0.40	≤0.40	≤0.10	≤0.015	≤0.015	Bal.

For the linear strategy, two parallel beads were deposited side by side with a step-over distance of 4.0 mm, which is defined as the distance between the centerlines of adjacent beads. Within each layer (intralayer strategy), deposition was unidirectional, meaning that the adjacent beads were deposited

with the same start and end points, as illustrated in Fig. 2a. Walls produced with the weaving strategy followed a triangular weave path, illustrated in Fig. 2b along with its defining parameters. Between successive layers (interlayer strategy), a bidirectional deposition sequence was adopted for both the linear and weaving strategies, alternating the start and end points of each layer to reduce the accumulation of excess material at arc start positions. All walls were 100 mm in length and were constructed by stacking five layers, incorporating a dwell period between layers to ensure adequate heat dissipation.

A wire feed speed (WFS) of 5.5 m/min was used in all experiments, which, through the built-in synergic control of the power source, corresponded to a welding current of 140 A and an arc voltage of 13.3 V.

For the linear case, the travel speed (TS) was 5 mm/s. The corresponding heat input was calculated using Eq. 1 and resulted in a value of 298 J/mm.

$$HI = \frac{\eta V I}{TS} \tag{1}$$

where

η = thermal efficiency (set to 0.8) [15]
V = arc voltage [V]
I = welding current [A]
TS = travel speed along the deposition direction [mm/s]

To provide the same total heat input per unit length of deposited wall for both strategies, the single oscillating track was deposited with a heat input of 596 J/mm, corresponding to the cumulative energy of the two linear passes. Accordingly, the traverse speed, TS_x, which is one of the two components of the weave motion and represents the longitudinal advancement of the torch along the wall, was adjusted to ensure this heat input and was therefore set to 2.5 mm/s, i.e., half of the 5 mm/s travel speed used in the linear case. Consequently, the actual travel speed along the triangular trajectory, TS_w, was calculated using the relationship given in Eq. 2 [14] and resulted in 14.2 mm/s:

$$TS_w = TS_x \sqrt{1 + \left(\frac{4A}{\lambda}\right)^2} \tag{2}$$

where

TS_x = weave traverse travel speed [mm/s]
A = weave path amplitude [mm]
λ = weave path wavelength [mm]

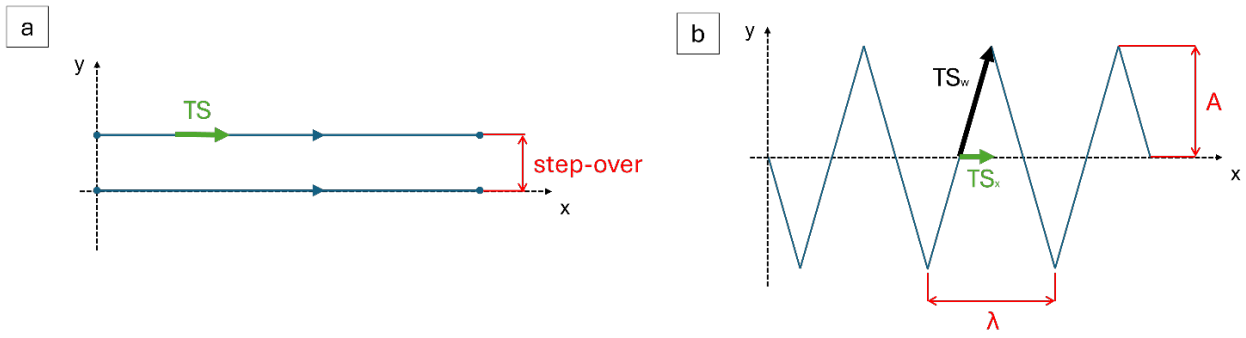

Fig. 2. Schematic representation of the deposition trajectories: (a) linear path and (b) triangular weave path used for material deposition.

As reported in the literature [13], a weaving frequency of $f = 1$ Hz was found to maintain a roughly constant penetration depth along the deposition direction and a more uniform thermal field. This value was therefore adopted in the present work. The wavelength of the weave, λ, was determined as the ratio of the longitudinal traverse speed, TS_x, to the weaving frequency, as depicted in Eq. 3, and was set at 2.5 mm:

$$\lambda = \frac{TS_x}{f} \quad (3)$$

The weave amplitude, $A = 3.5$ mm, was selected to replicate the effective width of two overlapping linear beads.
Table 2 summarizes the process parameters used for both the linear and weaving cases.

Table 2. Process parameters used for linear and weaving deposition strategies.

Deposition Strategy	WFS [m/min]	TS [mm/s]	Current [A]	Voltage [V]	CTWD [mm]	Weave parameters	
						Amplitude [mm]	Wavelength [mm]
Weave	5.5	14.2	140	13.3	15	3.5	2.5
Linear	5.5	5.0	140	13.3	15		

In a preliminary stage, single-layer depositions were produced and analyzed in terms of width and height in order to isolate the effect of the deposition trajectory on geometry and process stability, while minimizing the influence of layer stacking effects. Single-layer and multi-layer wall width and height were measured using a digital microscope at multiple locations along the deposition length to evaluate local geometric variations; the reported values represent the mean and standard deviation.
Surface waviness of the multi-layer walls was evaluated using a confocal optical microscope (Leica DCM3D). Multiple surface profiles were acquired at different positions from both lateral surfaces of each wall. The waviness parameters analyzed were the arithmetic mean waviness deviation, W_a, defined as the average absolute deviation from the mean line, and the total waviness height, W_t, defined as the vertical distance between the highest peak and the deepest valley within the evaluation length.
Vickers microhardness measurements were performed on cross-sections of the wall samples using a CV Instruments 2000 tester. The specimens were metallographically prepared according to the ASTM E3-11 standard, following sequential steps of cutting, mounting in resin, and grinding and polishing. Tests were carried out with a 500 g load, a dwell time of 15 s, and indentations spaced 1 mm apart along the wall height; the reported values correspond to the mean and standard deviation.

Results and Discussion

Fig. 3 presents the as-deposited walls examined in this study: (a) weave deposition and (b) linear deposition.

Fig. 3. Top view of the multi-layer walls produced with the two deposition strategies: (a) weave trajectory and (b) linear double-pass.

The comparison between single-layer depositions highlights distinct differences in both geometric dimensions and deposition stability, as summarized in Fig. 4. The weave single-pass strategy results in a slightly larger mean bead width (8.81 ± 0.07 mm) compared to the linear double-pass deposition (8.33 ± 0.18 mm), accompanied by a reduced mean height (4.40 ± 0.08 mm vs. 4.86 ± 0.20 mm). This behavior suggests a lateral redistribution of the molten material induced by the oscillatory motion of

the weave trajectory, which promotes spreading in the transverse direction at the expense of vertical buildup. More importantly, the weave strategy significantly reduces geometric variability. Standard deviations in width and height decrease by approximately 61% and 60%, respectively, compared to the linear double-pass case. This indicates a more stable and reproducible deposition process, with fewer local inconsistencies caused by the interaction between adjacent tracks and their thermal overlap.

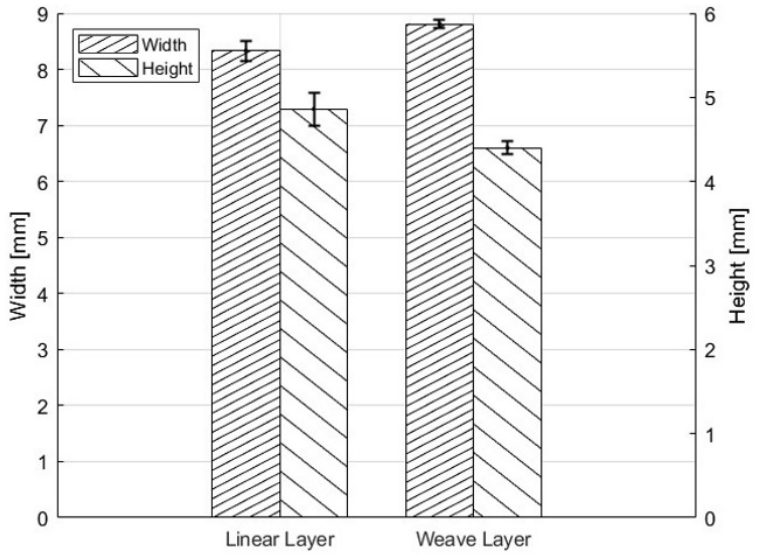

Fig. 4. Comparison of single-layer geometry for the two deposition strategies: mean width and height with corresponding standard deviations.

These trends are further reflected and amplified at the multi-layer scale, as illustrated in Fig. 5a. The weave-deposited wall exhibits a lower mean height (13.7 ± 0.1 mm) compared to the linear wall (15.7 ± 0.3 mm), bringing the final geometry closer to the nominal CAD target of 12 mm, while maintaining a comparable mean wall width (12.8 ± 0.3 mm vs. 12.6 ± 0.2 mm). The reduced height overshoot and smaller standard deviation indicate improved layer stacking consistency when using the weave strategy.

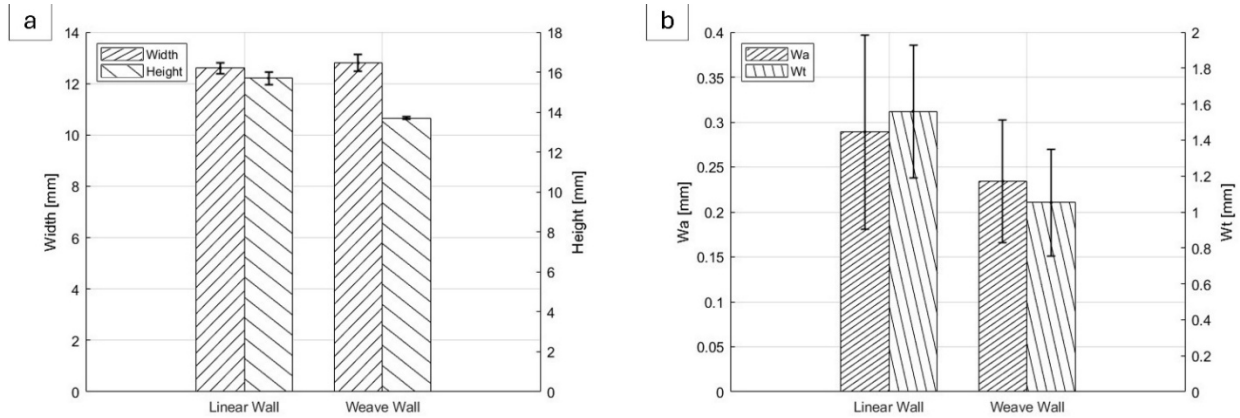

Fig. 5. Comparison of multi-layer walls geometry for the two deposition strategies: (a) mean width and height with standard deviations, and (b) mean waviness parameters (W_a and W_t) with standard deviations.

Surface quality is also markedly improved. As shown in Fig. 5b, both the average (W_a) and total (W_t) wall waviness are lower for the weave wall (W_a = 0.234 ± 0.068 mm; W_t = 1.052 ± 0.298 mm) than for the linear wall (W_a = 0.289 ± 0.108 mm; W_t = 1.559 ± 0.370 mm). Notably, the reduction in W_t (~33%) is more pronounced than that in W_a (~19%), indicating that the weave trajectory is particularly effective at suppressing extreme local deviations, which are often associated with transient process

instabilities or irregular layer stacking. The decrease in W_t is particularly significant, as it reduces the amount of material that must be removed during subsequent machining operations to achieve the desired final geometry. This highlights the practical advantage of the weave deposition strategy in producing near-net-shape parts and minimizing material waste.

Vickers microhardness measurements revealed subtle differences between the linear and weave walls (Fig. 6). The linear wall exhibited a mean microhardness of 235 ± 11 HV, while the weave-deposited wall showed a slightly lower mean value of 228 ± 3 HV. These hardness values are consistent with those reported in the literature for standard WAAM-CMT processes [10,16].

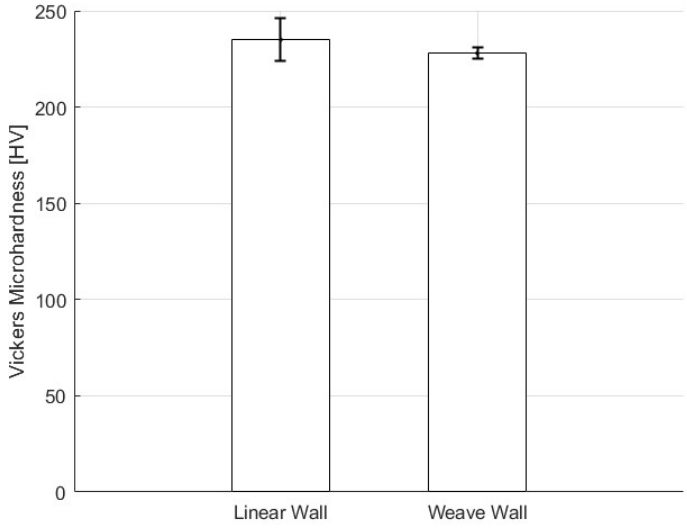

Fig. 6. Comparison of Vickers microhardness of multi-layer walls for the two deposition strategies.

The similarity in mean microhardness values suggests that the mechanical properties are primarily governed by the total heat input during deposition. Thus, under equivalent thermal conditions, the intrinsic microstructure of the material remains largely unaffected by the torch path. In contrast, the observed decrease in variability indicates that the deposition trajectory mainly affects the homogeneity of the material, mitigating local variability induced by thermal fluctuations and overlapping passes.

Conclusion

This study investigated the influence of deposition trajectory on the geometry, surface quality, and microhardness of multi-layer Inconel 625 walls produced by WAAM-CMT, comparing linear double-pass and triangular weave strategies under equivalent total heat input per unit length.

Walls produced with the weave trajectory exhibited lower height overshoot, comparable width, and significantly reduced surface waviness (W_a and W_t), indicating improved layer stacking consistency and more predictable wall geometry. Vickers microhardness measurements showed similar mean values for both strategies, confirming that mechanical properties are primarily governed by the total heat input, while the weave trajectory enhances material homogeneity by reducing local variability.

These findings demonstrate the importance of torch path design in optimizing WAAM-CMT process stability and part quality. Future work will focus on optimizing weave trajectories as a means to increase the deposition rate, thereby reducing production time while maintaining dimensional accuracy and surface quality. Additional investigations could also consider larger or more complex geometries and examine the relationship between trajectory design, microstructural features, and overall performance.

References

[1] C. Guo, M. Ying, H. Dang, R. Hu, and F. Chen, "Microstructural and intergranular corrosion properties of Inconel 625 superalloys fabricated using wire arc additive manufacturing," *Mater Res Express*, vol. 8, no. 3, p. 035103, Mar. 2021, doi: 10.1088/2053-1591/ABE977.

[2] A. N. M. Tanvir, M. R. U. Ahsan, C. Ji, W. Hawkins, B. Bates, and D. B. Kim, "Heat treatment effects on Inconel 625 components fabricated by wire + arc additive manufacturing (WAAM)—part 1: microstructural characterization," *The International Journal of Advanced Manufacturing Technology 2019 103:9*, vol. 103, no. 9, pp. 3785–3798, May 2019, doi: 10.1007/S00170-019-03828-6.

[3] R. S. Tanwar, P. Bhingole, and S. Jhavar, "A Comprehensive Review on Wire Arc Additive Manufacturing of Inconel Superalloys," *Lecture Notes in Mechanical Engineering*, pp. 113–129, 2025, doi: 10.1007/978-981-97-7114-1_10/FIGURES/7.

[4] G. Parmar, B. Tomar, S. Shiva, and A. K. Das, "Investigating the Effects of Deposition Strategies on the Performance of Inconel 625 in Wire Arc Additive Manufacturing," *Journal of Materials Engineering and Performance 2024 34:16*, vol. 34, no. 16, pp. 18227–18242, Dec. 2024, doi: 10.1007/S11665-024-10482-X.

[5] M. Rashid, S. Sabu, A. Kunjachan, M. Agilan, T. Anjilivelil, and J. Joseph, "'Advances in wire-arc additive manufacturing of nickel-based superalloys: Heat sources, DfAM principles, material evaluation, process parameters, defect management, corrosion evaluation and post-processing techniques,'" *International Journal of Lightweight Materials and Manufacture*, vol. 7, no. 6, pp. 882–913, Nov. 2024, doi: 10.1016/J.IJLMM.2024.05.009.

[6] M. Cheepu, C. I. Lee, and S. M. Cho, "Microstructural Characteristics of Wire Arc Additive Manufacturing with Inconel 625 by Super-TIG Welding," *Transactions of the Indian Institute of Metals 2020 73:6*, vol. 73, no. 6, pp. 1475–1479, Mar. 2020, doi: 10.1007/S12666-020-01915-X.

[7] G. H. S. F. L. Carvalho, A. T. Silvestri, G. Campatelli, and A. Squillace, "Effect of cooling strategies on Inconel 625 components produced by wire arc additive manufacturing," *International Journal of Advanced Manufacturing Technology*, vol. 133, no. 7–8, pp. 3631–3646, Aug. 2024, doi: 10.1007/S00170-024-13978-X/TABLES/7.

[8] A. El Hassanin, G. Campatelli, R. Sepe, A. T. Silvestri, and A. Squillace, "Effect of energy input on fatigue crack growth behavior of titanium alloy Ti6Al4V made by WAAM-CMT," *Fatigue Fract Eng Mater Struct*, vol. 47, no. 4, pp. 1466–1481, Apr. 2024, doi: 10.1111/FFE.14257.

[9] M. Bhuvanesh Kumar, P. Sathiya, and S. M. Senthil, "A critical review of wire arc additive manufacturing of nickel-based alloys: principles, process parameters, microstructure, mechanical properties, heat treatment effects, and defects," *Journal of the Brazilian Society of Mechanical Sciences and Engineering 2023 45:3*, vol. 45, no. 3, pp. 164-, Feb. 2023, doi: 10.1007/S40430-023-04077-1.

[10] O. M. Akselsen, R. Bjørge, H. W. Ånes, X. Ren, and B. Nyhus, "Microstructure and Properties of Wire Arc Additive Manufacturing of Inconel 625," *Metals 2022, Vol. 12, Page 1867*, vol. 12, no. 11, p. 1867, Nov. 2022, doi: 10.3390/MET12111867.

[11] Q. Jiang *et al.*, "Microstructure and Mechanical Properties of Thick-Walled Inconel 625 Alloy Manufactured by Wire Arc Additive Manufacture with Different Torch Paths," *Adv Eng Mater*, vol. 23, no. 1, p. 2000728, Jan. 2021, doi: 10.1002/ADEM.202000728.

[12] J. Zhao *et al.*, "Influence of deposition path strategy on residual stress and deformation in weaving wire-arc additive manufacturing of disc parts," *Journal of Materials Research and Technology*, vol. 30, pp. 2242–2256, May 2024, doi: 10.1016/J.JMRT.2024.03.226.

[13] L. Palmeira Belotti, J. A. W. van Dommelen, M. G. D. Geers, W. Ya, and J. P. M. Hoefnagels, "Influence of the printing strategy on the microstructure and mechanical properties of thick-walled wire arc additive manufactured stainless steels," *J Mater Process Technol*, vol. 324, p. 118275, Mar. 2024, doi: 10.1016/J.JMATPROTEC.2023.118275.

[14] J. Bultman and C. Saldaña, "Effects of weave path parameters on the geometry of wire arc additive manufactured features," *The International Journal of Advanced Manufacturing Technology 2022 124:7*, vol. 124, no. 7, pp. 2563–2577, Dec. 2022, doi: 10.1007/S00170-022-10546-Z.

[15] Y. Zhao, F. Chen, S. Cao, C. Chen, and R. Xie, "Effect of CMT Welding Heat Input on Microstructure and Properties of 2A14 Aluminum Alloy Joint," *Metals 2022, Vol. 12, Page 2100*, vol. 12, no. 12, p. 2100, Dec. 2022, doi: 10.3390/MET12122100.

[16] C. Zhang *et al.*, "On the Effect of Heat Input and Interpass Temperature on the Performance of Inconel 625 Alloy Deposited Using Wire Arc Additive Manufacturing–Cold Metal Transfer Process," *Metals 2022, Vol. 12, Page 46*, vol. 12, no. 1, p. 46, Dec. 2021, doi: 10.3390/MET12010046.